Kinetics and Catalysis, Vol. 46, No. 2, 2005, pp. 260–268. Translated from Kinetika i Kataliz, Vol. 46, No. 2, 2005, pp. 278–287.

Luminescence of Al_2O_3 Crystal Modifications Excited by the ArF Excimer Laser

V. N. Snytnikov, V. O. Stoyanovskii, V. A. Ushakov, and V. N. Parmon

Boreskov Institute of Catalysis, Siberian Division, Russian Academy of Sciences, Novosibirsk, 630090 Russia

Received December 29, 2003

Abstract—Luminescence spectra induced by a high-power UV laser pulse in the excitation range of extraneous ions in alumina can provide valuable information on this compound. The laser-induced luminescence (LIL) technique markedly extends the capabilities and the area of application of photoluminescence spectroscopy. Luminescence measurements in the red spectral region enable one to detect octahedrally coordinated Cr^{3+} ions at concentrations down to 10^{-7} wt % in metastable alumina modifications. The fact that the Cr^{3+} luminescence line occurs in different positions in the α- and θ-alumina allows LIL spectroscopy to be used in phase and elemental analysis of thin surface layers and in surface temperature measurements when studying the microstructure of heterogeneous catalysts under real pressures and in a real gas medium, including *in situ* measurements.

Characterization of the surface and subsurface layers of catalysts is the most important task of most studies in heterogeneous catalysis. A wide variety of physicochemical methods are used for this purpose [1]. However, gas pressures typical of chemical reactors allow application of optical spectroscopic methods only, including *in situ* ones. Among them, photoluminescence spectroscopy in the visible and UV regions has provided important information concerning the structure of active surface sites in oxide catalysts [2, 3]. These catalysts include numerous systems based on ZrO_2, SiO_2, Al_2O_3, MgO, and TiO_2 [2–4].

The optical properties of many of these oxides, metal sulfides, and some other compounds, including phosphors, are determined by metal activators, which are often present in trace amounts (10^{-3}–10^{-6} wt % or below) [5]. In some cases, the luminescence of oxides is due to lattice defects such as *F*-centers [6] or the excitation of lattice oxygen O^{2-}, as in vanadium oxo complexes on ZrO_2, SiO_2, Al_2O_3, and MgO [4]. It is noteworthy that surface *F*-centers, metal activators, and surface oxo complexes can serve as active sites in catalytic reactions.

Photoluminescence spectroscopy is very sensitive, but it is not universal. It is mainly used in the determination of active components and impurities at concentrations as low as <0.1 wt % [2, 3]. Without affecting the chemical properties of the sample, concentration can be measured to a depth of $\delta \approx \lambda/4\pi\kappa$, where κ is the complex part of the refractive index and λ is the wavelength of light absorbed. When studying layer composition and structure, adsorption, and catalysis, one can record luminescence from surface layers with δ between tens and hundreds of nanometers at the vacuum UV edge (near the fundamental absorption region), where $\lambda \approx 200$ nm and $\kappa \approx 1$ or below. However, in the 180–350 nm range, which accommodates the excitation bands of the above and many other oxides having surface and bulk active sites, the spectral intensity of tube emitters is low. As a consequence, luminescence intensity is also low. At the same time, the existence and availability of high-power excimer UV lasers (involving ArF, KrF, XeCl, etc.) and sensitive spectroscopic CCD chambers for registration of radiation make it possible to experimentally evaluate the potential of the laser-induced luminescence (LIL) method in catalytic applications [7]. Here, we report such evaluation based on LIL data for alumina, which is widely used in industrial catalysis.

Catalysts may contain the following alumina modifications: γ, η, χ, δ, θ, κ, and α. Most alumina specimens contain traces of chromium, whose ions can intensively luminesce. Note that traces of Cr^{3+} in Al_2O_3 do not affect $\gamma\text{-}Al_2O_3 \longrightarrow \alpha\text{-}Al_2O_3$ transition kinetics. Therefore, study of the electronic spectra of chromium oxo complexes can provide information concerning the crystal structure of the environment of the chromium ion, the coordination of this ion, the presence of quenchers, surface temperature, solid-state transitions, etc. Important results can be obtained by examining the very narrow "ruby" luminescence lines of Cr(III), which are assigned to a spin-forbidden (quartet–doublet) transition. These lines are observed for most chromium oxo complexes, primarily for ruby, which is among the best known $\alpha\text{-}Al_2O_3$ single crystals. Ruby contains Cr^{3+} ions and is the material on which classical laser systems are based. It was expected that metastable aluminum oxides, which are produced from various modifications of aluminum hydroxide differing in structure and composition (amorphic hydroxide, pseudoboehmite, boehmite, bayerite, and hydrargillite), would be characterized by different LIL spectra, depending on the synthetic conditions. For alumina

0023-1584/05/4602-0260 © 2005 MAIK "Nauka/Interperiodica"

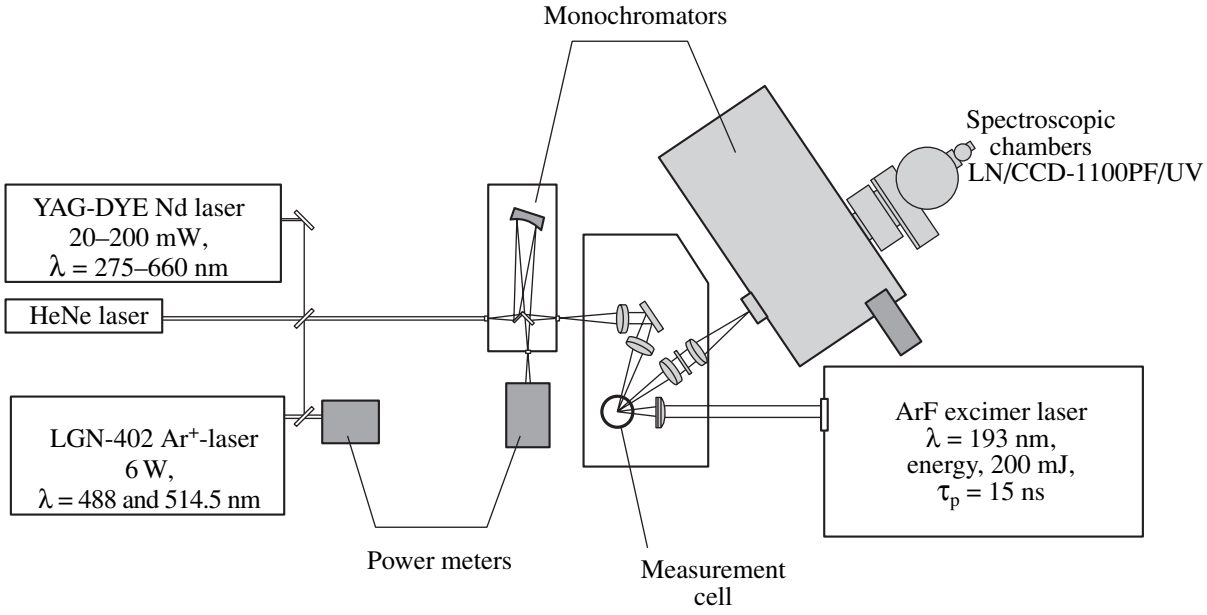

Fig. 1. Schematic of the spectroscopic setup for studying laser-induced luminescence from ultrafine powders and monolith catalysts.

specimens prepared by sol–gel processing, primarily α- and θ-phases, excitation of luminescence with a HeNe or Ar^+ ion laser [8] gave emission spectra with different edge regions [9]. The high excitation efficiency of these continuous-wave lasers is due to the comparatively large absorption cross sections for their wavelengths.

The purpose of this study is to evaluate the possibilities that are opened up by LIL excited with pulsed ArF-laser radiation with a wavelength of 193 nm ($h\nu$ = 6.45 eV) to obtain emission spectra in the visible and UV regions. This method is tested on real supports, including various alumina phases.

EXPERIMENTAL

Measurements were carried out on a spectroscopic bench (Fig. 1) designed at the Boreskov Institute of Catalysis, Siberian Division of the Russian Academy of Sciences. Luminescence was excited with an ArF laser (pulse duration, τ_p = 15 ns; pulse energy, up to 200 mJ) and an LGN-402 Ar^+ laser (Russia; wavelength, 514.5 nm). Radiation power density on the sample surface could be varied between 0.001 and 50 MW/cm^2 using a calibrated radiation attenuator equipped with a KU-1 quartz lens with a focal distance of $f \approx$ 85–125 mm. Laser radiation was controlled by measuring the energy of each pulse. The beam was focused on the surface of a powder sample placed in a quartz cell. LIL radiation was focused on the entrance slit of an MDR-12 fast monochromator (LOMO, Russia) and an ICCD IRY 1024 G/R (Spectroscopy Instruments, Germany) or an LN/CCD-1100PF/UV (Princeton Instruments, United States) spectroscopic chamber, using a KU-1 quartz convertible spherocylindrical lens with a focal distance of 85 mm. At wavelengths shorter than 120 nm, LIL spectra were recorded using a single laser pulse with an exposure time of 30 ms. Since luminescence spectra are very sensitive to surface impurities, including organic ones, special care was taken of the cleanness of cells and samples, and it was ascertained that the cell itself did not luminesce. Scattered laser radiation was filtered using a dielectric mirror with a transmittance of 5% at λ = 193 nm and a transmission bandwidth of 20 nm. In order to eliminate radiation of higher diffraction orders for λ ≥ 275 nm, we used PS-11 and ZhS-4 standard glass filters. Wavelengths between 190 and 800 nm were measured with an accuracy of 0.1 nm using neon- and mercury-tube lines as references. To measure the characteristic time of luminescence and study luminescence decay kinetics, we used an FEU-100 photomultiplier (Russia) with a Tektronix TDS224 oscilloscope (United States). The optical cell was designed so that it was possible to maintain sample temperature in the wide range of 77–800 K.

The materials characterized by LIL spectroscopy included characterized alumina powders and pellets with different phase compositions (Table 1) provided by the authors of earlier publications [10, 11]. Furthermore, we studied single crystals of ruby (Cr^{3+} α-Al_2O_3) and optical colorless sapphire (α-Al_2O_3). These powders consisted of particles with a typical diameter of 1–50 μm (the mean particle diameter was 30–40 μm). The pellets were irregularly shaped, had a size of 0.25–0.75 mm, and contained small amounts of finer fractions. The size of primary crystallites was 4–50 nm or larger, depending on alumina modification. The hydroxides used in the preparation of alumina con-

Table 1. Alumina powders examined

Specimen		Calcination temperature, °C	Preparation conditions and characteristic crystallite size (δ)
no.	composition		
1	α-Al_2O_3	1200	Obtained by amorphization of pseudoboehmite (γ + χ) for 3 h in a catalytic heat generator; δ ≈ 500 Å
2	θ-Al_2O_3 with traces of the α-phase	1200	Obtained by calcination of boehmite for 50 h; δ ≥ 200 Å
3	θ-Al_2O_3 with traces of the α-phase	1000	Obtained by calcination of reprecipitated pseudoboehmite for 5 h; δ ≥ 200 Å
4	κ-Al_2O_3	950	Obtained by calcination of natural gibbsite for 6 h; δ ≈ 160–200 Å
5	δ-Al_2O_3	900	Obtained by calcination of boehmite for 50 h; δ ≈ 160–200 Å
6	δ-Al_2O_3	900	Obtained by calcination of pseudoboehmite for 50 h; δ ≈ 160–200 Å
7	γ-Al_2O_3	600	Obtained by calcination of pseudoboehmite (prepared from reprecipitated gibbsite) for 4 h; δ ≈ 50 Å

tained the following impurities (wt %): Si, 0.57; Fe, 0.024; Cr, 0.0063; and Na, <0.001. The total amount of the other impurities did not exceed 0.001 wt %. According to X-ray fluorescence analysis, the silicon and iron contents of sapphire crystals were below 0.5 and 0.1 wt %, respectively, close to the lower measurement limits of VRA-20 and SPRUT-001 instruments. No other impurities were found above the detection limit of 0.001 wt %.

X-ray powder diffraction was carried out on URD-63 and HZG-4 (Germany) diffractometers. The diffraction patterns from Al_2O_3 are presented in Fig. 2, and the phase composition data derived from these patterns are listed in Table 1. As is noted in an earlier publication [12], the diffraction patterns of δ- and θ-Al_2O_3 obtained from boehmite and pseudoboehmite differ fundamentally in peak positions and intensities at d/n = 2.02–1.91 Å (2θ ≈ 44.9°–46.6°) and d/n = 2.85–2.59 Å

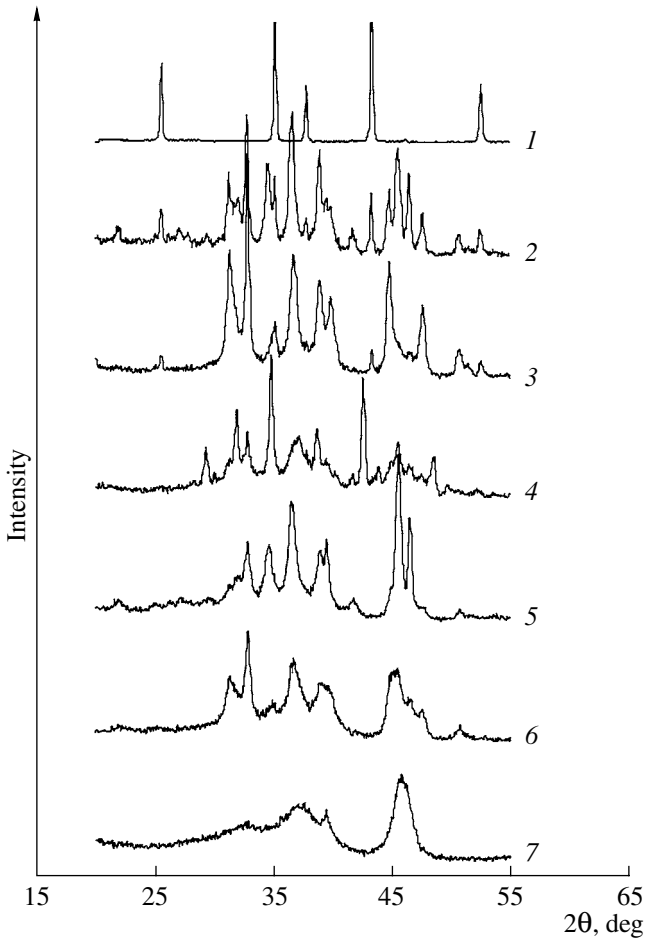

Fig. 2. X-ray diffraction patterns from alumina specimens *1*–*7* (see Table 1) at 2θ = 20°–55° (CuK_α radiation).

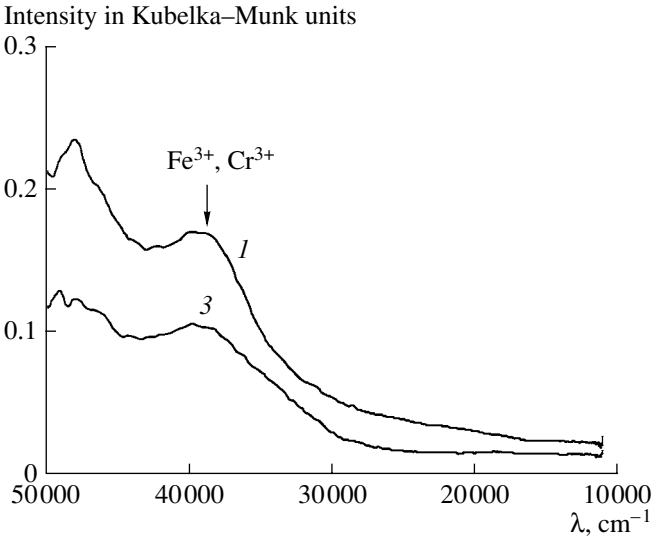

Fig. 3. Diffuse reflectance electronic spectra of alumina specimens *1* and *3*.

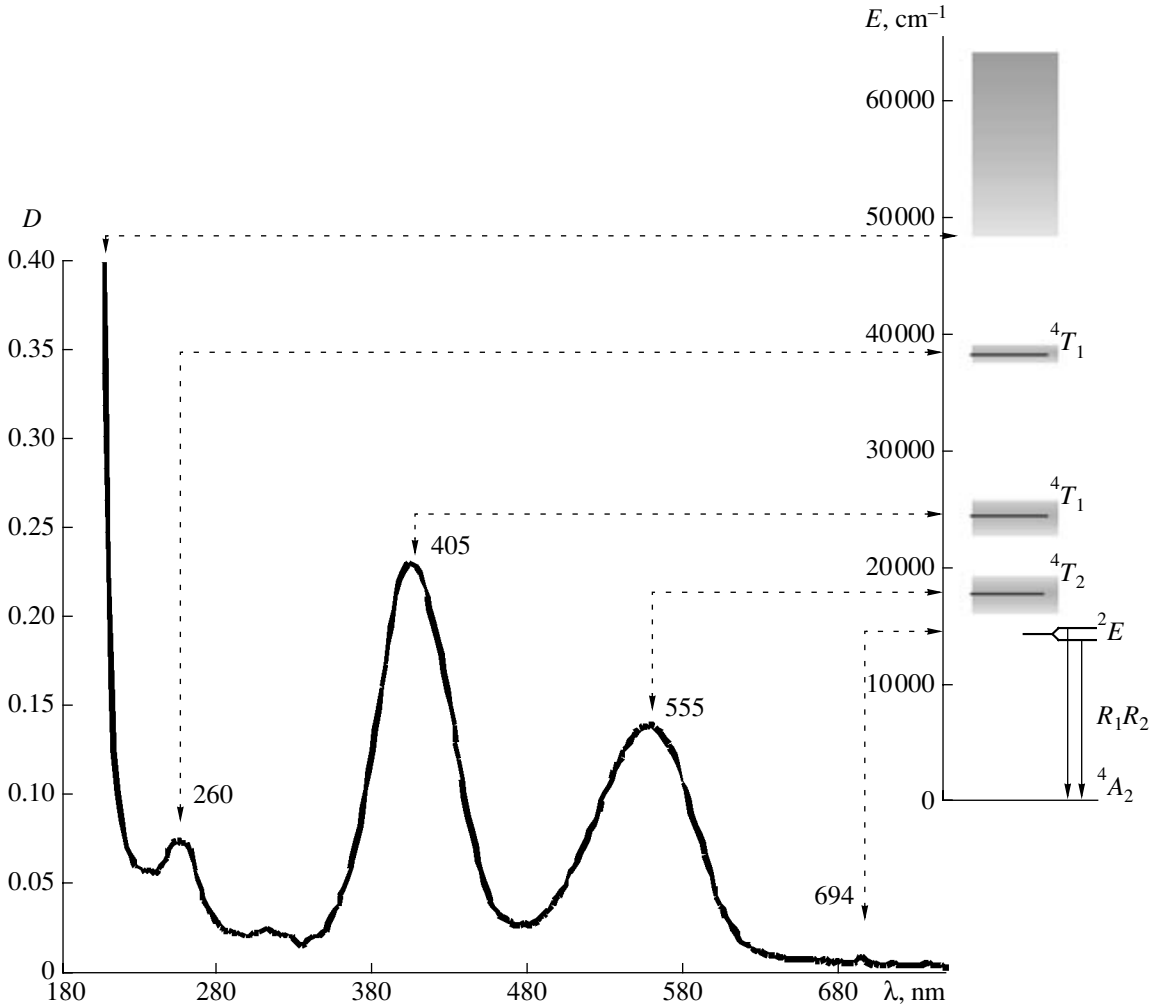

Fig. 4. Absorption spectrum of ruby containing 0.0148 wt % foreign ions. Transitions due to four spin quartets ($^4A_2(t^3)$, $^4T_2(t^2e)$, and two $^4T_1$) and the lowest radiating metastable level ^2E are shown.

($2\theta \approx 31°$–$35°$) (Fig. 2), suggesting that these oxides are individual phases.

Diffusion reflectance and absorption spectra were recorded on a UV-VIS-4501 spectrophotometer (Shimadzu, Japan). The charge-transfer absorption band at 37000 cm^{-1} (Fig. 3) for samples *1* and *3*, which is due to Fe^{3+} ions, masked the absorption band of the Cr^{3+} ion, and the *d*–*d* transition band of the chromium ion fell below the measurement limit of the instrument. X-ray photoelectron spectroscopy (ESCALAB HB instrument, United Kingdom) revealed traces of C, Ca, Cl, Si, and Na in the subsurface layers of all samples.

RESULTS

As a reference, we used a ruby single crystal, whose absorption spectrum is presented in Fig. 4 together with the scheme of the main electronic levels. The concentration of Cr^{3+} ions in this sample (0.0148 wt %) was measured as absorbance in the region of *R*-lines [13]. The absorption spectrum of Cr^{3+} ions in ruby is due to four spin quartets: $^4A_2(t^3)$, $^4T_2(t^2e)$, and two $^4T_1$ ones. The broad U [$^4A_2(t^3) \longrightarrow {}^4T_2(t^2e)$] and Y [$^4A_2 \longrightarrow a^4T_1$] bands in the visible region, which are responsible for the red color of ruby, and the $^4A_2 \longrightarrow b^4T_1$ band in the UV region are due to constant-spin ($\Delta S = 0$) transitions from the ground level $^4A_2$. For the short-wavelength charge-transfer band at $\lambda \le 200$ nm, the quantum yield of luminescence was $\eta(\lambda) = 0.85$–0.95 [14]. This means radiative transition of most of the electrons from excited levels to the metastable level ^2E.

According to our data, the quantum yield of luminescence for Cr^{3+} impurity ions is invariable until the radiation power density at the target is $Q = 0.1$ MW/cm^2 ($\lambda = 193$ nm; $\tau_p = 15$ ns). The quantum yield is independent of Cr^{3+} concentration if this concentration is below ~0.145 wt % [15]. The upper estimate of the change in surface temperature is $\Delta T \approx 5$–6 K ($Q = 0.1$ MW/cm^2;

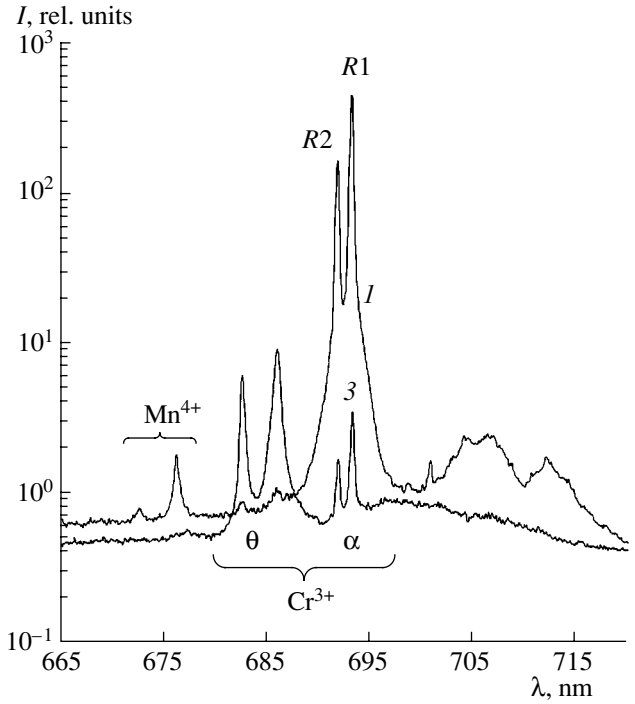

Fig. 5. Luminescence spectra of α-Al_2O_3 (specimen *1*) and θ-Al_2O_3 + α-Al_2O_3 (specimen *3*) excited with an ArF pulsed laser (λ = 193 nm). Sample temperature is 77 K; Q = 0.1 MW/cm^2.

absorption coefficient, $\alpha_c = 10^4$ cm^{-1}; $\tau_p = 15$ ns; thermal diffusivity, $\chi = 0.14$ cm^2/s), and the characteristic cooling time is $\tau \approx 1/(\alpha_c^2 \chi) \approx 70$ ns. Therefore, as soon as a few tens of microseconds after the laser pulse, the effect of sample heating on spectroscopic data can be neglected at the power density specified above and below. Furthermore, surface temperature can be derived from, e.g., *R*-line intensity ratios.

The LIL spectra of α-Al_2O_3 (specimen *1*) and (θ + α)-Al_2O_3 (specimen *3*) at λ = 670–710 nm, T = 77 K, and a radiation power density of Q = 0.1 MW/cm^2 are shown in Fig. 5. Under these conditions, our setup revealed no difference between the *R*1 and *R*2 lines for ruby and specimen *1* (α-Al_2O_3). These intense lines, positioned at λ = 693.5 and 692.0 nm, are labeled with α in Fig. 5. They were also observed for a colorless optical sapphire (α-Al_2O_3) single crystal. At the same time, the luminescence spectra of specimens *1* and *3* are fundamentally different. A specific feature of the spectrum of (θ + α)-Al_2O_3 (*1*) is that it contains not only an α line but also two intense lines at λ = 682.6 and 685.9 nm (labeled with θ). These lines were observed for all specimens in which θ-alumina had been identified by X-ray diffraction. However, the spectrum of specimen *1* also shows weak lines due to the θ-phase, although the amount of this phase is beyond the sensitivity of the XRD method. Furthermore, the LIL spectrum of specimen *1* exhibits *R* lines due to Mn^{4+} impurity ions, for which *R*-doublet splitting Δν is 80 cm^{-1} [16].

Figure 6 plots the intensity of the α line for α-Al_2O_3 (*1*) and of the α and θ lines for (θ + α)-Al_2O_3 (*3*) as a function of temperature. Elevating the temperature shifts these lines to longer wavelengths. The temperature dependence of these lines indicates luminescence quenching between 700 and 800 K. After a laser pulse $t \le 10$ ms, line intensity decreased according to the

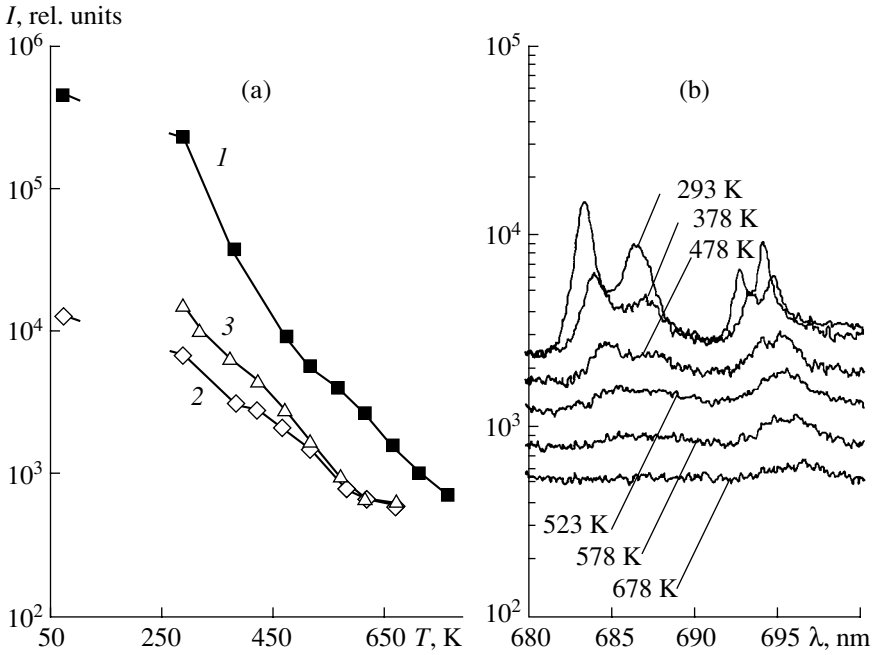

Fig. 6. (a) Intensity of the α line in the luminescence spectrum of specimen *1* and of the θ line in the spectra of specimens *2* and *3* as a function of temperature. (b) Spectra of specimen *3* at various temperatures. Exposure time is 30 ms.

hyperbolic law $I = I_0/(1 + (I_0\beta)^{1/2}t)^2$, which means recombination decay [5] with rate constants of $\beta = 2.9 \times 10^{-8}$ ($\pm 2 \times 10^{-9}$) cm^3/s for the α line and $\beta = 3.5 \times 10^{-8}$ ($\pm 2 \times 10^{-9}$) cm^3/s for the θ line at 293–300 K.

The luminescence spectra of specimens *2–7* at T = 77 K, λ = 670–710 nm, and $Q \approx 0.1$ MW/cm^2 are presented in Fig. 7. The spectrum of γ-Al_2O_3 (specimen *7*) shows a weak diffuse band at both room temperature and 77 K. The spectra of specimens containing κ- or δ-Al_2O_3, exhibit α and θ lines and a diffuse band at λ = 680–730 nm. The intensities of these lines and diffuse band grow as the calcination temperature is increased in going from γ- to δ- and then θ-alumina. The short-wavelength boundary of the diffuse band is the same for all phases and is situated at the broad θ line.

The spectra of specimens that have been obtained from boehmite or pseudoboehmite and contain δ-Al_2O_3 show weak θ lines, and the spectrum of the specimen that has been obtained from gibbsite and contains κ-Al_2O_3 shows both α and θ lines (Table 2). The luminescence spectra of specimens *2* and *5* (synthesized from boehmite) differ from those of specimens *3* and *6* (obtained from pseudoboehmite) in that they contain two lines at λ = 690 and 702.3 nm. The line at 702.3 nm is observed only at 77 K. The line at 690 nm is characterized by approximately the same luminescence quenching temperature as the α and θ lines (700–800 K).

From R line intensity data for specimens with different phase compositions and the same initial Cr^{3+} content, we were able to derive α- and θ-Al_2O_3 content data not only for specimens in which the α- and θ-phases had been found by XRD but also for specimens in which these phases were undetectable by this method. These data are listed in Table 2. α-Phase content was measured relative to specimen *1*, which was pure α-Al_2O_3 according to XRD data. θ-Phase content was measured against specimen *2*, which contained >98% θ-Al_2O_3.

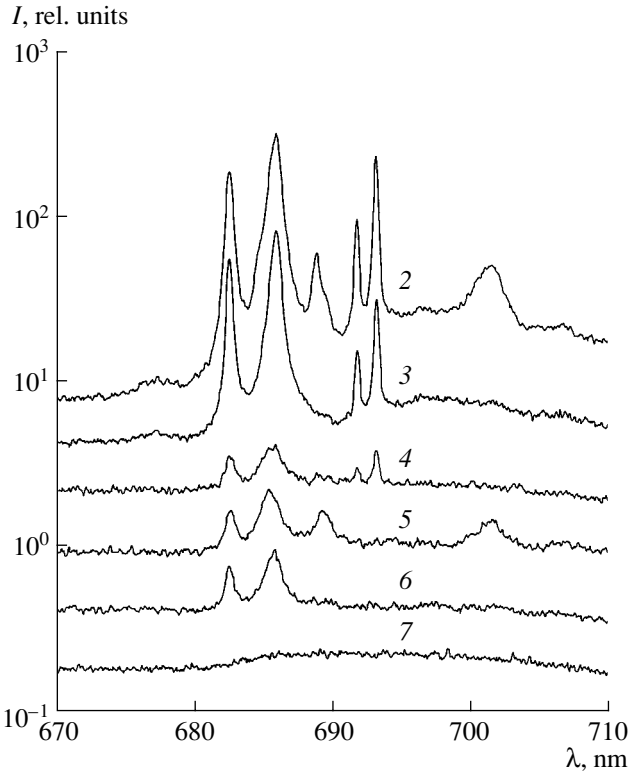

Fig. 7. Luminescence spectra of specimens *2–7* excited with an ArF pulsed laser (λ = 193 nm). Sample temperature is 77 K; Q = 0.1 MW/cm^2. Spectra are shifted along the ordinate axis by multiplying I by 15, 9, 3, 1.5, 0.6, and 0.3, respectively.

Increasing radiation power density may cause laser desorption and sublimation of matter from the surface. Interaction between the vaporized substance and the gas medium lowers the radiation ionization thresholds of the desorption and sublimation products. However, these products are transparent to ArF laser radiation and do not prevent it from penetrating to the solid. It was

Table 2. Luminescence lines and α- and θ-phase contents (wt %) for alumina powders (chromium content, 0.0063 wt %)

Specimen		Calcination temperature, °C	Observed lines and α and θ-phase contents*
no.	composition		
1	α-Al_2O_3	1200	α (100) and θ (0.3)
2	θ-Al_2O_3 with traces of the α-phase	1200	α (7.2) and θ (98.5)**
3	θ-Al_2O_3 with traces of the α-phase	1000	α (1.5) and θ (32.4)
4	κ-Al_2O_3	950	Weak lines α (0.24) and θ (3.2)
5	δ-Al_2O_3	900	Weak lines θ (4.8)**
6	δ-Al_2O_3	900	Weak lines θ (4.0)
7	γ-Al_2O_3	600	Weak diffuse band
8	ruby α-Al_2O_3		α

* α: 692.9 and 694.3 nm; θ: 683.6 and 687.0 nm.

** Lines at 690 and 702.3 nm are also observed.

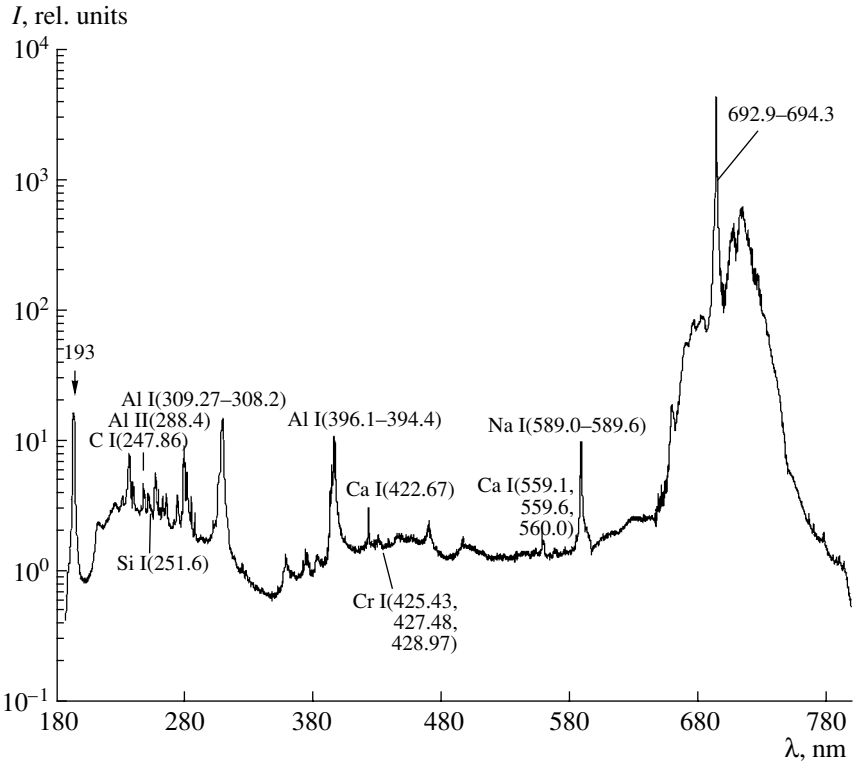

Fig. 8. Luminescence spectrum of ruby (α-Al_2O_3 + 0.0148 wt % Cr^{3+}) excited with an ArF pulsed laser (λ = 193 nm). Sample temperature is 293 K; Q = 50 MW/cm^2.

therefore expected that, at high power densities, the emission spectrum would be a superposition of the luminescence spectrum of the solid and the spectrum of the excited products of laser desorption.

Indeed, between 200 and 800 nm, the emission spectra of ruby (Fig. 8), α-Al_2O_3 powder (specimen *1*; Fig. 9), and specimens *2–7*, all recorded at room temperature and $Q \approx 50$ MW/cm^2, are very similar to the luminescence spectra recorded at radiation power densities below 0.1 MW/cm^2 and T = 350–400 K. However, the former contain extra lines due to neutral and ionized elements. Between 200 and 600 nm, there are identified lines common to all specimens, including ruby. These are the most intense doublets due to aluminum atoms Al I at 309.27–308.2 nm [$3s^2$ (^{1}S)$3p$ – $3s^2$ (^{1}S)$3d$; ^{2}P – ^{2}D] and 396.1–394.4 nm [$3s^2$ (^{1}S)$3p$ – $3s^2$ (^{1}S)$4s$; ^{2}P – ^{2}S], a doublet due to sodium atoms Na I at 589.0–589.6 nm ($3s$ – $3p$; ^{2}S – ^{2}P), and a line due to singly charged aluminum ion Al II at 281.6 nm ($3s3p$ – $3s4s$). Lines due to C, Ca, Si, and Cr are also identified in the spectrum of ruby. The presence of these elements in the surface layer is confirmed by XPS. At a radiation power density below ~5 MW/cm^2, no lines due to neutral or ionized aluminum or other elements are observed.

DISCUSSION

The power density of the pulsed radiation exciting luminescence was varied between 0.001 and 50 MW/cm^2 up to values seven to nine orders of magnitude higher than the power density attainable with standard spectrofluorimeters. For $Q < 0.1$ MW/cm^2, the LIL spectrum of alumina is linear with respect to excitation intensity. Starting at $Q \approx 20$ MW/cm^2, ions appear in the desorption and sublimation product near the sample surface.

Radiation with λ = 193 nm is absorbed in a thinner Al_2O_3 surface layer than radiation caused by excitation in the visible region. According to the literature [17], the linear absorption coefficient for Al_2O_3 at λ = 193 nm is $\alpha_c = (3 \times 10^3 – 1.0 \times 10^4)$ cm^{-1} and absorption nonlinearity is $\beta_c = (5 \times 10^1 – 1.4 \times 10^2)$ mJ/cm^3. This means that the absorption depth is between $\delta \approx 0.4$–1.0 μm at an exposure dose of H = 0.01 J/cm^2 and $\delta \approx$ 90–200 nm at H = 1 J/cm^2. The radiation absorption cross section of single-crystal ruby with [Cr^{3+}] ≈ 0.01 wt % at λ = 193 nm is determined by impurities, including Cr^{3+} ions. For these ions, the absorption cross section at λ = 193 nm is larger by more than one order of magnitude than the absorption cross section in the visible region [14]. For 99.5% Al_2O_3, the complex part of the refractive index is $\kappa \approx 0.5$ [18] and the absorption depth at small exposure doses ($\ll$0.01 J/cm^2) is $\delta \approx \lambda/4\pi\kappa \approx 30$ nm. So small doses of pulsed radiation do

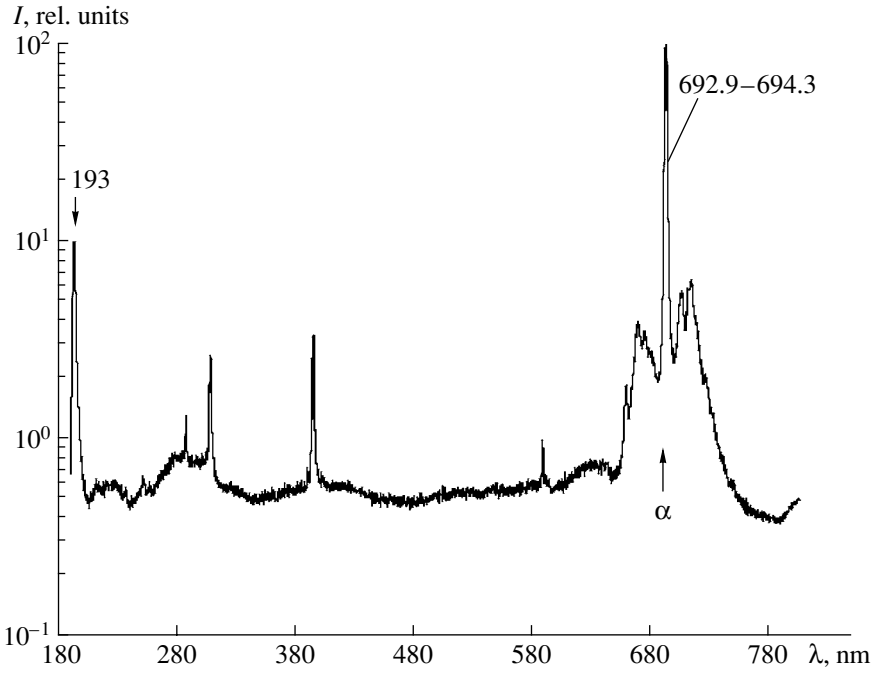

Fig. 9. Luminescence spectrum of alumina powder (specimen *1*) excited with an ArF pulsed laser (λ = 193 nm). Sample temperature is 293 K; Q = 20 MW/cm^2.

not heat the sample, eliminating the problem of thermal stabilization when recording spectra at cryogenic or other temperatures.

In our experiments, luminescence arose from radiative transitions of photoexcited d^3 electrons of foreign, octahedrally coordinated Cr^{3+} ions in α- and θ-Al_2O_3, which are the most perfectly ordered alumina phases. The presence of a broad, diffuse luminescence band and the absence of intense lines in the spectra of the γ-, δ-, and κ-Al_2O_3 specimens examined may be due to the high degree of disorder in these phase and the presence of an OH^- group in the first coordination sphere of the Cr^{3+} ion.

The positions of the α and θ lines coincide with their positions observed in other studies (see, e.g., [8, 9]) in which alumina contained Cr^{3+} ions and luminescence was excited with an Ar^+ ion laser operated at λ = 514.5 nm. Our experiments demonstrated that, at comparable exposure doses, exciting specimen *1* (α-Al_2O_3) with an Ar^+ laser at λ = 193 nm allows luminescence intensity to be increased by more than one order of magnitude [7].

Furthermore, the luminescence spectrum of specimen *1* (Fig. 9) shows a band at 660–740 nm, which is characteristic of vibronic transitions in ruby [19], occurring near the intense ruby luminescence lines at 694.3 and 692.9 nm (Fig. 8). This band is labeled with α in Fig. 9. In these spectra, which were recorded at Q = 20 MW/cm^2, the positions and intensity ratios of the $R1$ and $R2$ lines and other features in the red region are similar to the corresponding features of the spectra obtained at Q = 0.1 MW/cm^2 and a sample temperature of 320–370 K. No changes in the LIL spectrum of alumina were observed at power densities below 20 MW/cm^2 and total exposure doses up to 70 J/cm^2.

Radiation power densities above 20 MW/cm^2 cause layer-by-layer cleaning of the surface through desorption and sublimation. In this case, LIL spectra are successively taken from different depths of the sample under real gas pressures [7].

The spectra of most of the other low-temperature alumina modifications, whose samples were shaped as granules of pellets with a size of about 1 cm (these data re not presented in Tables 1 and 2), generally showed lines characteristic of high-temperature (α- and θ-) modifications of Al_2O_3. Some γ-phase specimens were the rare exception. These high-temperature phases occur on outer surfaces and are undetectable by standard XRD techniques. In some cases, after the pellets were ground, the α- and θ-phases did not show themselves any longer. The fact that the α- and θ-phases were detected in the outer layers of specimens obtained at low calcination temperatures is explained by the high sensitivity of the LIL method. In our nondestructive spectroscopic measurements, it was possible to detect Cr^{3+} in α-Al_2O_3 down to a concentration of 10^{-7} wt % using a single laser pulse at T = 293 K and Q = 0.1 MW/cm^2.

Iron-family ions with an incomplete 3d shell (Ti^{3+}, Cr^{3+}, V^{3+}, Mn^{4+}, Fe^{3+}, and Ni^{3+}) substitute for Al^{3+} ions in the α-Al_2O_3 lattice, giving rise to strong absorption lines between 6 and 7 eV [20]. Since these metals are

important for catalysis, it is necessary to reveal the possibilities opened up by the LIL method in the study of alumina supports and catalysts containing the above ions. Another promising line of investigation is applying LIL to high concentrations of foreign metals.

CONCLUSIONS

The above results demonstrate that luminescence excited by a high-power UV laser pulse in the excitation range of impurity ions in alumina is a promising sensitive source of valuable information on this compound, which is commonly used in catalysis. The luminescence of other compounds can be excited using the UV radiation of existing excimer or other lasers. The LIL method markedly extends the capabilities of photoluminescence spectroscopy. It enables one to study catalysts under real reactor conditions, under which conventional photoluminescence spectroscopy is hardly applicable.

LIL spectroscopy in combination with other physicochemical methods is useful in investigation of the crystal environment of iron-family ions, the coordination extraneous metal ions, and active sites in the surface layers of fine oxide powders and monolith oxide catalysts. Recording a luminescence spectrum in the red region allowed the Cr^{3+} ion at a concentration level of at least 10^{-7} wt % to be identified in metastable modifications of alumina.

The fact that the Cr^{3+} luminescence line occurs in different positions in the α- and θ-alumina allows LIL spectroscopy to be used in phase and elemental analysis of thin surface layers and in surface temperature measurements when studying the microstructure of heterogeneous catalysts under real pressures and in a real gas medium, including *in situ* measurements.

ACKNOWLEDGMENTS

We thank our colleagues from the Boreskov Institute of Catalysis, namely, A.S. Ivanova, Z.R. Ismagilov, and O.P. Krivoruchko, for providing alumina specimens and A.I. Boronina for XPS measurements. This work was sponsored through the "Support to Leading Scientific Schools" program (grant NSh-1484.2003.3) and by the Russian Foundation for Basic Research (grant no. 02-03-33351a). We are grateful to G.M. Zhidomirov, the manager of the latter grant, for helpful discussion of some issues.

REFERENCES

1. Moiseev, I.I., *Kinet. Katal.*, 2000, vol. 41, no. 1, p. 5.
2. Anpo, M. and Che, M., *Adv. Catal.*, 2000, vol. 44, p. 119.
3. Pott, G.T. and Stork, W.H.J., *Catal. Rev.—Sci. Eng.*, 1975, vol. 12, p. 163.
4. Fenin, V.A. and Shvets, V.A., *Dokl. Akad. Nauk SSSR*, 1980, vol. 252, p. 1427.
5. Gurvich, A.M., *Vvedenie v fizicheskuyu khimiyu kristallofosforov* (Introduction to the Physical Chemistry of Crystalline Phosphors), Moscow: Vysshaya Shkola, 1982.
6. Feofilov, P.P. and Arkhangel'skaya, V.A., *Izv. Akad. Nauk SSSR, Ser. Fiz.*, 1981, vol. 45, p. 302.
7. Snytnikov, V.N. and Stoyanovskii, V.O., *Dokl. Akad. Nauk*, 2003, vol. 392, p. 501.
8. Carturan, G. and Di Maggio, R., *J. Mater. Sci.*, 1990, vol. 25, p. 2705.
9. Wen, Q. and Lipkin, D.M., *J. Am. Ceram. Soc.*, 1998, vol. 81, p. 3345.
10. Ivanova, A.S., Litvak, G.S., Kryukova, G.N., Tsybulya, S.V., and Paukshtis, E.A., *Kinet. Katal.*, 2000, vol. 41, no. 1, p. 137.
11. Ismagilov, Z.R., Shkrabina, R.A., and Koryabkina, N.A., *Alyumosilikatnye nositeli: proizvodstvo, svoistva i primenenie v kataliticheskikh protsessakh zashchity okruzhayushchei sredy. Analiticheskii obzor* (Aluminosilicate Supports for Catalysts: Production, Properties, and Environmental Applications—A Review), Novosibirsk: Sib. Otd. Ross. Akad. Nauk, 1998.
12. Ushakov, V.A. and Moroz, E.M., *Kinet. Katal.*, 1985, vol. 26, no. 4, p. 963.
13. Grum-Grzhimailo, S.V., Pasternak, L.B., Sviridov, D.T., *et al.*, in *Spektroskopiya kristallov* (Spectroscopy of Crystals), Moscow: Nauka, 1966, p. 168.
14. Morgenshtern, Z.L. and Nevstruev, V.V., *Opt. Spektrosk.*, 1966, vol. 20, p. 837.
15. Gevorkyan, V.A., Madatyan, K.A., Kochinyan, E.A., *et al.*, in *Spektroskopiya kristallov* (Spectroscopy of Crystals), Moscow: Nauka, 1970, p. 280.
16. Valyashko, E.G., Grum-Grzhimailo, S.V., Kutovoi, I.M., *et al.*, in *Spektroskopiya kristallov* (Spectroscopy of Crystals), Moscow: Nauka, 1966, p. 211.
17. Apel, O. and Mann, K., *Appl. Opt.*, 2000, vol. 39, p. 3165.
18. Zukic, M. and Torr, D.G., *Appl. Opt.*, 1990, vol. 29, p. 4284.
19. Nelson, D.F. and Sturge, M.D., *Phys. Rev.*, 1965, vol. 137, no. 4A, p. A1117.
20. Tippins, H.H., *Phys. Rev. B: Condens. Matter*, 1970, vol. 1, p. 126.